J Mol Model (2012) 18:559–568
DOI 10.1007/s00894-011-1085-5

ORIGINAL PAPER

Interactions between $Al_{12}X$ (X = Al, C, N and P) nanoparticles and DNA nucleobases/base pairs: implications for nanotoxicity

Peng Jin · Yongsheng Chen · Shengbai B. Zhang · Zhongfang Chen

Received: 4 November 2010 / Accepted: 7 April 2011 / Published online: 6 May 2011

Abstract The interactions between neutral $Al_{12}X(I_h)$ (X = Al, C, N and P) nanoparticles and DNA nucleobases, namely adenine (A), thymine (T), guanine (G) and cytosine (C), as well as the Watson−Crick base pairs (BPs) AT and GC, were investigated by means of density functional theory computations. The $Al_{12}X$ clusters can tightly bind to DNA bases and BPs to form stable complexes with negative binding Gibbs free energies at room temperature, and considerable charge transfers occur between the bases/BPs and the $Al_{12}X$ clusters. These strong interactions, which are also expected for larger Al nanoparticles, may have potentially adverse impacts on the structure and stability of DNA and thus cause its dysfunction.

Keywords Aluminum cluster · DNA · Nucleobase · Base pair · Density functional theory · Interaction · Nanotoxicity

Introduction

Nanoparticles (NPs) are "fickle" and have diverse biological effects depending on their size, chemical composition, shape, surface charge density, hydrophobicity, and aggregation. These complex effects make it extremely difficult to understand nanoparticles' toxicities in different situations. As a result, nanotoxicity remains poorly understood, and a systematic approach to assessing the potential toxicology of nanomaterials is still non-existent [1, 2].

Experimentalists have made great progress (for very recent reviews, see [3–13]), especially in evaluating the toxicity of basic nanomaterials in vitro [14]. In stark contrast, computational studies aimed at understanding the toxicity of NPs are scarce [15–25], but are giving us rather instructive information. For example, by molecular dynamics (MD) simulations, Zhao et al. [16] suggested that C_{60} can bind tightly to single-strand (ssDNA) or double-strand DNA (dsDNA) in aqueous solution and significantly affect the nucleotides. Zhao further found that three typical water-soluble C_{60} derivatives can associate strongly with ssDNA segments and that they exhibit different binding features depending on their different functional groups [17].

Given the rapid growth of nanotechnologies and the massive production of NPs in the near future, it is impossible to test the biological effects of all the nanoscale products in vivo. Thus, fundamental theoretical research on nanotoxicity prediction is urgently required. Probing inter-

Electronic supplementary material The online version of this article (doi:10.1007/s00894-011-1085-5) contains supplementary material, which is available to authorized users.

P. Jin
Wuhan Center for Magnetic Resonance,
State Key Laboratory of Magnetic Resonance and Atomic and Molecular Physics, Wuhan Institute of Physics and Mathematics,
Chinese Academy of Sciences,
Wuhan 430071, China

P. Jin (✉) · Z. Chen (✉)
Department of Chemistry, University of Puerto Rico,
San Juan, PR 00931, USA
e-mail: pengjin@wipm.ac.cn

Z. Chen
e-mail: Zhongfangchen@gmail.com

Y. Chen
School of Civil and Environmental Engineering,
Georgia Institute of Technology,
Atlanta, GA 30332, USA

S. B. Zhang
Department of Physics, Applied Physics, and Astronomy,
Rensselaer Polytechnic Institute,
Troy, NY 12180, USA

actions between NPs and biological systems is the first critical step in understanding and ultimately predicting nanotoxicity.

Aluminum, a widely used metal, caught our great attention. People are exposed to aluminum in daily life through food and water consumption as well as through the use of many commercial products, such as antacids and antiperspirants. High aluminum concentrations in the human body can lead to anemia, bone disease, and dementia [26–28]. Besides, aluminum may be associated with neurological disorders such as dialysis encephalopathy, Parkinson's dementia, and, especially, Alzheimer's disease [29, 30]. Very recent in vitro experimental studies show that Al NPs impair the cell's natural ability to respond to a respiratory pathogen regardless of NP composition (Al or Al_2O_3) [31].

Not surprisingly, theoretical and experimental studies have been performed to address the interactions between aluminum and nucleobases/base pairs or nucleotides. For example, using photoionization efficiency spectra, Pedersen et al. [32] found that Al atoms can stabilize an unusual tautomer of guanine that is incompatible with the formation of Watson-Crick base pairs (BPs). The theoretical studies of Mazzuca et al. [22] indicate that aluminum ions and nucleobases, as well as the corresponding nucleotides, can form stable complexes with large binding energies. Single aluminum atoms and trications were found to have high affinity to nucleic acid bases and monophosphate nucleotides [22, 33, 34]. However, all these studies considered only Al atoms and trications—no study involving Al NPs has been reported to the best of our knowledge.

Upon entering cells, Al NPs may coordinate with DNA and RNA nucleobases and disrupt their formation, replication and cleavage, and consequently, cause adverse effects to human health. To understand the possible toxicity of aluminum-based NPs in the human body, a detailed study on the interactions between Al NPs and DNA nucleobases as well as the corresponding BPs is urgently needed.

Choosing an appropriate NP model is crucial to the investigation of the bonding mechanism between Al NPs and DNA. Bare Al_{13} is a well-known magic cluster that has gained much attention for many years. Its neutral form is one electron deficient compared to the closed 40-electron shell given by the jellium model [35]. The icosahedral configuration is generally considered the most energetically favorable structure of neutral Al_{13}. Substituting the inner aluminum atom of Al_{13} (I_h) with a tetravalent atom such as C (or Si) leads to a closed shell configuration, just as in a noble gas superatom [36–39]. On the other hand, doping with an atom with five valence electrons such as P (or N) results in a super alkali-metal atom with one extra electron [39, 40]. Having similar sizes and shapes but diverse redox properties, these doped $Al_{12}X$ clusters (X = Al, C, N and P) are ideal models of Al-based NPs. A comparison of these four NPs will also provide information on how the properties of NP binding to biosystems may change with different electronic configurations.

Thus, in this work, we used neutral bare $Al_{12}X$ clusters as simple NP models to investigate theoretically their interactions with adenine (A), thymine (T), guanine (G) and cytosine (C) as well as AT and GC pairs. The goal was to shed light on the possible biotoxicity caused by different NP configurations. Issues such as the geometries, electronic properties and binding Gibbs free energies of the complexes of bases/BPs with $Al_{12}X$ clusters are addressed. The mechanisms of Al NP binding as well as potential adverse effects on human biosystems are also suggested.

Computational methods

First, full geometry optimizations without symmetry constraints were carried out using the M05-2X functional [41] with the standard 6-31G* basis set. The M05-2X functional has exhibited outstanding performance in evaluating the geometries and energies of systems involving DNA bases [41, 42], and the optimized geometries of $Al_{12}X$ clusters at this level also agree well with earlier studies [43]. Several possible binding sites on nucleobases and BPs (Fig. 1, individual bases have the same numbering schemes) were considered to interact with $Al_{12}X$ (I_h) clusters, although in practice some sites may be blocked by sugar residues (ssDNA) or by intermolecular hydrogen bonds (dsDNA). All isomers were characterized as local minima by harmonic vibrational frequency analysis at the same theoretical level after the optimization. Then, the lowest-energy structures were reoptimized

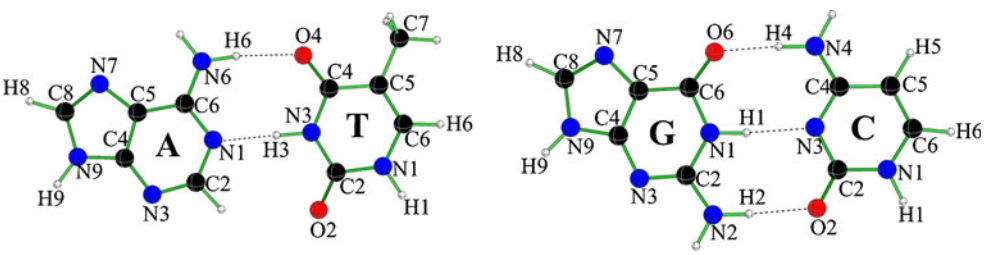

Fig. 1 Geometries and numbering schemes for the Watson-Crick base pairs AT [adenine (A)–thymine (T)] and GC [guanine (G)–cytosine (C)]

with the larger 6-311+G* basis set using polarizable continuum model (PCM) [44] to take the effect of solvent (water) into account. Charge distributions were studied with the aid of the natural bond order (NBO) analysis of Weinhold et al. [45].

To evaluate the binding strength at room temperature, we computed the binding Gibbs free energy (ΔG_b, 298.15 K and 1 atm) at the M05-2X/6-311+G* level of theory. ΔG_b is defined as the difference in Gibbs free energy between a base/BP-$Al_{12}X$ complex and the separate base/BP and Al cluster (i.e., $\Delta G_b = G$(base/BP-$Al_{12}X$) − [G(base/BP) + G($Al_{12}X$)]). The computed ΔG_b values were adjusted for basis set superposition error (BSSE) using the Boys-Bernardi counterpoise correction scheme [46]. The Gaussian 03 package was employed throughout our density functional theory (DFT) computations [47]. The molecular orbitals were plotted using the gOpenmol program [48, 49].

Results and discussion

Geometries and energetics of base-$Al_{12}X$ complexes

In DNA nucleobases, electron-rich N and O atoms are conventionally favored for metal binding, while the exocyclic amino groups in A, G and C can bind with metals only after deprotonation or in tautomer structures [50, 51]. Thus, we considered the initial isomers by binding $Al_{12}X$ to the principal sites (either endocyclic N atoms or exocyclic carbonyl O atoms) in bases, namely, N1, N3, N7 of adenine, O2, O4 of thymine, N3, N7, O6 of guanine, and O2, N3 of cytosine. The lowest-energy complexes screened from the M05-2X/6-31G* optimized geometries (Table S1 summarizes all isomers, see Supporting Information) were reoptimized at the M05-2X/6-311+G* level of theory using PCM, and are presented in Fig. 2.

Adenine has three endocyclic nitrogen atoms (namely N1, N3 and N7, Fig. 1), all of which are potential sites for metal binding. The complexes with $Al_{12}X$ bound to the N3 site of adenine are the most favorable energetically (Table S1). The nearest base-$Al_{12}X$ distances (R_{b-Al}) have the order A-Al_{13} (1.96 Å) < A-$Al_{12}N$ (1.98 Å) < A-$Al_{12}C$ (2.00 Å) = A-$Al_{12}P$ (2.00 Å) (Fig. 2). The BSSE corrected ΔG_b values at 298.15 K (Table 1, −16.0, −7.3, −16.9 and −14.5 kcal mol^{-1} for A-Al_{13}, A-$Al_{12}C$, A-$Al_{12}N$ and A-$Al_{12}P$, respectively) also suggest substantial interactions between adenine and the $Al_{12}X$. Clearly, A-$Al_{12}C$ has a relatively larger ΔG_b due to the closed shell configuration of the metal cluster.

For T-$Al_{12}X$ complexes, the isomers with the metal bound to the O2 atom of thymine have more favorable energies. In contrast, σ bonding to O4 was preferred in other reports involving single Al atoms in either neutral or ionic form [22, 52]. T-$Al_{12}X$ has the same ΔG_b and similar R_{b-A1} orders as A-$Al_{12}X$, i.e., for ΔG_b, T-$Al_{12}N$ (−12.5 kcal mol^{-1}) < T−Al_{13} (−10.9 kcal mol^{-1}) < T-$Al_{12}P$ (−9.6 kcal mol^{-1}) < T-$Al_{12}C$ (5.2 kcal mol^{-1}), and for R_{b-A1}, T-Al_{13} (1.84 Å) = T-$Al_{12}C$ (1.84 Å) < T-$Al_{12}N$ (1.86 Å) < T−$Al_{12}P$ (1.87 Å). However, the T-$Al_{12}X$ complexes have larger ΔG_b values than A-$Al_{12}X$.

The G-$Al_{12}X$ complexes binding guanine via O6 sites are all most favorable energetically. Basically, their ΔG_b values are all slightly smaller than those of A-$Al_{12}X$ and T-$Al_{12}X$. G-$Al_{12}P$ has the smallest ΔG_b (−19.7 kcal mol^{-1}), followed by G-$Al_{12}N$ (−17.3 kcal mol^{-1}). Although relatively large, the ΔG_b of G-$Al_{12}C$ is still considerable (−8.7 kcal mol^{-1}). Like that of A-$Al_{12}X$, the R_{b-Al} obeys the order of G-Al_{13} (1.82 Å) < G-$Al_{12}N$ (1.84 Å) < G-$Al_{12}C$ (1.85 Å) = G-$Al_{12}P$ (1.85 Å). Earlier studies proposed that a single Al atom or ion can bridge the O6 and the N7 atoms to form a stable structure [22, 32, 53]. As in the case of the G-$Al_{12}X$ complexes studied here, the metal binding to the O6 site may distort GC pairing and lead to the formation of globular DNA [54–57].

Generally, neutral cytosine favors N3 or O2 sites for binding with metals, depending on the nature of the metal and steric factors. When an $Al_{12}X$ cluster attaches to cytosine, Al_{13}, $Al_{12}C$ and $Al_{12}N$ prefer the O2 site, whereas $Al_{12}P$ forms a bicoordinated complex with the N3 and O2 sites, adopting a similar binding pattern to the complex between cytosine and a single Al atom (or its cation and anion) [22, 33].

Energetically, the most stable complex is C-$Al_{12}P$ (ΔG_b −21.3 kcal mol^{-1}), followed by C-$Al_{12}N$ (−18.3 kcal mol^{-1}), C-Al_{13} (−16.9 kcal mol^{-1}) and C-$Al_{12}C$ (−9.5 kcal mol^{-1}). These complexes have the smallest ΔG_b values among all the base-$Al_{12}X$ complexes studied here. A large binding energy of cytosine-Al (neutral atom) was observed experimentally and suggested theoretically [33, 34]. R_{b-Al} has the order of C-Al_{13} (1.81 Å) < C-$Al_{12}N$ (1.82 Å) < C-$Al_{12}C$ (1.83 Å) < C-$Al_{12}P$ (1.89 Å, 1.98 Å). The high stability of C-$Al_{12}P$ may be due to the two-fold intra-cluster interactions (from both N–Al and O–Al bonds).

From the above, we can draw the following conclusions:

(1) $Al_{12}X$ clusters prefer to bind to O atoms over N atoms in the bases. A similar behavior was also found when hard transition metals interact with DNA bases [58].

(2) Based on ΔG_b, the relative affinities of individual bases to the same $Al_{12}X$ cluster are ordered as T < A < G < C. In addition, ΔG_b has the order $Al_{12}P$ < $Al_{12}N$ (or $Al_{12}N$ < $Al_{12}P$) < Al_{13} < $Al_{12}C$ for the same bases. Thus, T-$Al_{12}C$ has the largest ΔG_b (5.2 kcal mol^{-1}) of all the base-$Al_{12}X$ complexes. The special case of C-$Al_{12}P$ features bicoordination and the smallest binding Gibbs free energy (−21.3 kcal mol^{-1}).

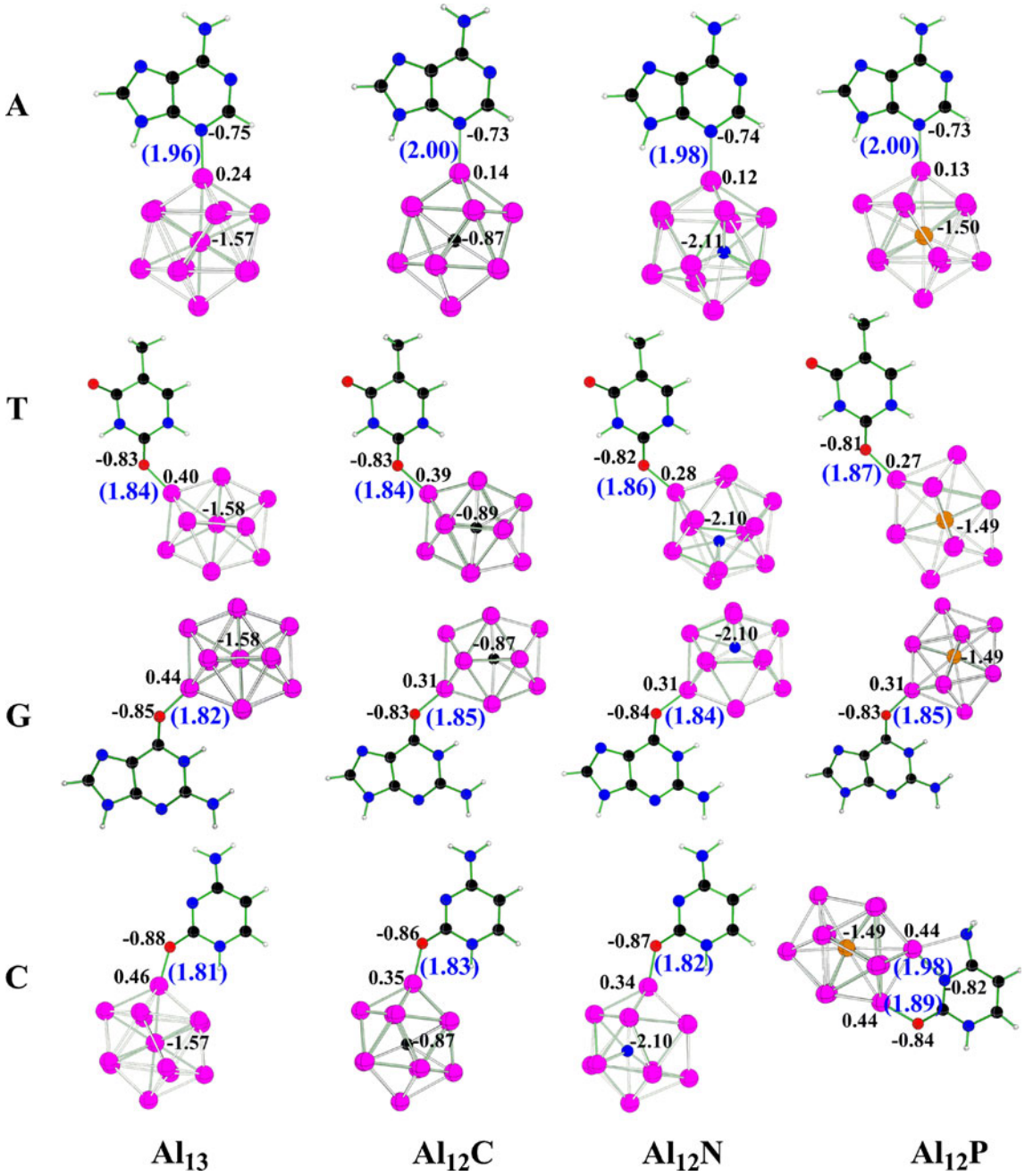

Fig. 2 Optimized geometries of the lowest-energy complexes of DNA base-$Al_{12}X$ and computed natural bond order (NBO) charges for selected atoms at the M05-2X/6-311+G* level of theory. *Black* C, *red* O, *blue* N, *white* H, *pink* Al, *yellow* P. The nearest base-$Al_{12}X$ distances ($R_{b\text{-}Al}$, unit: Å) and charges are given in *blue* (in parentheses) and *black*, respectively

(3) Basically, R_{b-Al} has the order $Al_{13} < Al_{12}N < Al_{12}C < Al_{12}P$ for a single base and the order C < G < T < A for a single $Al_{12}X$. Thus, C-Al_{13} and A-$Al_{12}P$ have the shortest (1.81 Å) and the longest R_{b-Al} values (2.00 Å), respectively, among all the base-$Al_{12}X$ complexes. The shortest R_{b-Al} is attributed to the interaction between the lone pairs (from O or N atoms) on the bases and the electron-deficient outer orbitals of Al_{13}.

Geometries and energetics of BP-$Al_{12}X$ complexes

Similar patterns are apparent in the interactions between DNA BPs and $Al_{12}X$ clusters. Figure 3 illustrates the optimized structures of the complexes at the M05-2X/6-311+G* level of theory, while Table 1 summarizes the corresponding binding Gibbs free energies, ΔG_b. In the AT-$Al_{12}X$ complexes, Al_{13}, $Al_{12}C$ or $Al_{12}N$ bound to the N3 site of the adenine moiety have the lowest energy, whereas $Al_{12}P$

Table 1 Basis set superposition error (BSSE)-corrected binding Gibbs free energies ΔG_b (kcal mol^{-1}) of the base/BP-$Al_{12}X$ complexes computed at the M05-2X/6-311+G* level of theory

	Al_{13}	$Al_{12}C$	$Al_{12}N$	$Al_{12}P$
A	−16.0	−7.3	−16.9	−14.5
T	−10.9	5.2	−12.5	−9.6
G	−15.8	−8.7	−17.3	−19.7
C	−16.9	−9.5	−18.3	−21.3
AT	−14.5	−8.0	−22.3	−11.0
GC	−10.2	−4.0	−17.9	−16.2

prefers the O2 site of thymine (Table S2). In the case of GC-$Al_{12}X$ complexes, however, all four $Al_{12}X$ clusters prefer binding at the O6 and the N7 sites of the guanine moiety in a bridging fashion.

The BSSE-corrected ΔG_b values (−14.5, −8.0, −22.3 and −11.0 kcal mol^{-1} for AT-Al_{13}, AT-$Al_{12}C$, AT-$Al_{12}N$ and AT-$Al_{12}P$, respectively) suggest that the interaction between AT and $Al_{12}N$ is the strongest, while that between AT and $Al_{12}C$ is the weakest. The $R_{BP\text{-}Al}$ values of AT-Al_{13} and AT-$Al_{12}C$ are exactly the same as the $R_{b\text{-}Al}$ values of the corresponding A-$Al_{12}X$ complexes (1.96 and 2.00 Å, respectively), while the $R_{BP\text{-}Al}$ values of AT-$Al_{12}N$ (1.97 Å) and AT-$Al_{12}P$ (1.82 Å) decrease by 0.01 and 0.05 Å compared to the $R_{b\text{-}Al}$ values of A-$Al_{12}N$ (1.98 Å) and T-$Al_{12}P$ (1.87 Å), respectively. AT-$Al_{12}C$ has the longest $R_{BP\text{-}Al}$ and the largest ΔG_b because of the high chemical stability of $Al_{12}C$, while AT-$Al_{12}P$ and AT-$Al_{12}N$ have the shortest $R_{BP\text{-}Al}$ and the smallest binding Gibbs free energy, respectively.

With the $Al_{12}X$ clusters simultaneously bridging O6 and N7 of guanine, GC-Al_{13}, GC-$Al_{12}C$, GC-$Al_{12}N$ and GC-$Al_{12}P$ all have considerable ΔG_b values (−10.2, −4.0, −17.9 and −16.2 kcal mol^{-1}, respectively). The average bond lengths (to O6 and N7 sites) are 1.94, 1.97, 1.95 and 1.93 Å, respectively, for Al_{13}, $Al_{12}C$, $Al_{12}N$ and $Al_{12}P$, leading to the order: GC-$Al_{12}P$ < GC-Al_{13} < GC-$Al_{12}N$ < GC-$Al_{12}C$. Among these, GC-$Al_{12}N$ has the strongest binding strength and is energetically the most stable.

Intermolecular hydrogen bonds play an important role in the stabilities of BPs and their associated complexes. Thus, we computed the intermolecular hydrogen bond distances in the BP-$Al_{12}X$ complexes in comparison with pure BPs (Table 2). Our computed hydrogen-bond parameters in BPs are consistent with previous high-level computations [59, 60].

For AT-Al_{13}, AT-$Al_{12}C$ and AT-$Al_{12}N$, with respect to normal AT, the N6(A)···O4(T) hydrogen bond distances decrease slightly, by 1.3%, whereas the N1(A)···N3(T) distances increase by 2.4%. However, these two hydrogen bonds become shorter (by 3.7 and 3.5%, respectively) in the AT-$Al_{12}P$ complex. Interestingly, in binding with the $Al_{12}P$, H3 (T) approaches the adenine moiety more closely [H3(T)–N1(A) and H3(T)–N3(T) are 1.05 and 1.74 Å, respectively, see Fig. 3]. In the GC-$Al_{12}X$ complexes, the hydrogen bond distances of O6(G)···N4(C) increase dramatically (by 8.5, 7.4, 8.8 and 4.9% for GC-Al_{13}, GC-$Al_{12}C$, GC-$Al_{12}N$ and GC-$Al_{12}P$, respectively), whereas most of the N1(G)···N3(C) distances are enlarged slightly

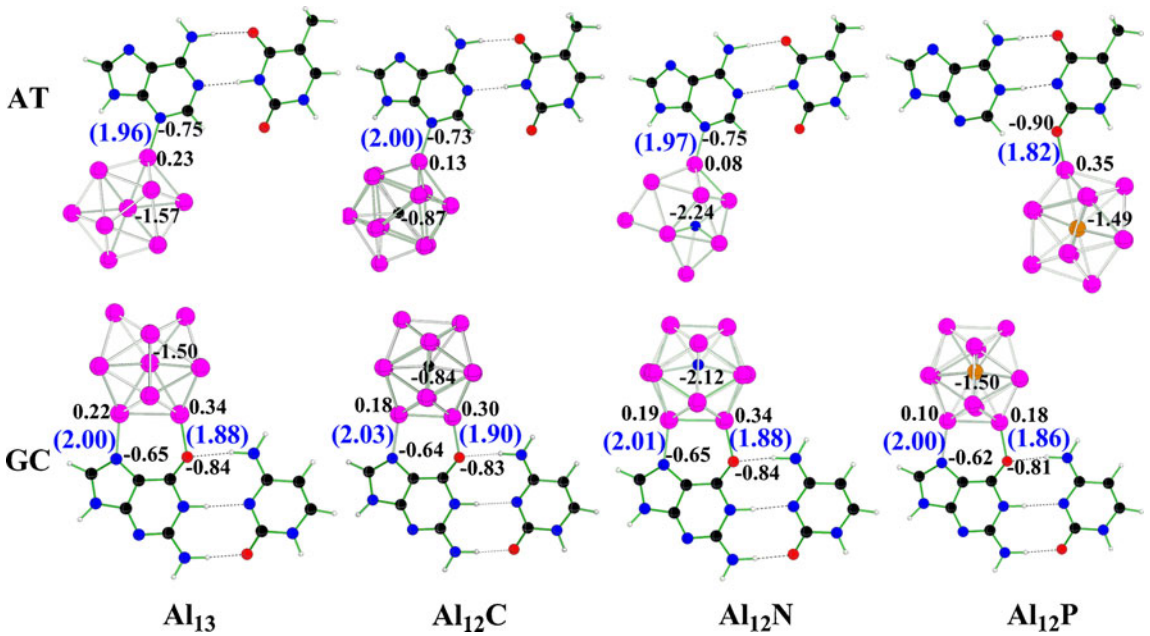

Fig. 3 Optimized geometries of the lowest-energy isomers of base pair (BP)-$Al_{12}X$ complexes and computed NBO charges for selected atoms at the M05-2X/6-311+G* level of theory. Coloring and labeling scheme as in Fig. 2

Table 2 Computed hydrogen bond lengths (Å) and BSSE corrected base–base interaction energies ΔE (kcal mol^{-1}) in BP-$Al_{12}X$ complexes at the M05-2X/6-311+G* level of theory[a]. *BP* Base pair

		BP	BP−Al_{13}	BP−$Al_{12}C$	BP−$Al_{12}N$	BP−$Al_{12}P$
AT	N6(A)···O4(T)	2.98	2.94 (−1.3)	2.94 (−1.3)	2.94 (−1.3)	2.87 (−3.7)
	N1(A)···N3(T)	2.89	2.96 (+2.4)	2.96 (+2.4)	2.96 (+2.4)	2.79 (−3.5)
	ΔE	−14.8	−14.7 (−0.7)	−14.7 (−0.7)	−14.6 (−1.4)	−97.7 (+560.1)
GC	O6(G)···N4(C)	2.84	3.08 (+8.5)	3.05 (+7.4)	3.09 (+8.8)	2.98 (+4.9)
	N1(G)···N3(C)	2.97	3.00 (+1.0)	3.01 (+1.3)	2.93 (−1.3)	2.99 (+0.7)
	N2(G)···O2(C)	2.94	2.79 (−5.1)	2.80 (−4.8)	2.83 (−3.7)	2.82 (−4.1)
	ΔE	−30.4	−31.8 (+4.6)	−31.8 (+4.6)	−30.3 (−0.3)	−31.2 (+2.6)

[a] Variations from the free BPs are given in parentheses (%)

(except GC-$Al_{12}N$). In contrast, the N2(G)···O2(C) bonds shorten considerably (by 5.1, 4.8, 3.7 and 4.1% for GC-Al_{13}, GC-$Al_{12}C$, GC-$Al_{12}N$ and GC-$Al_{12}P$, respectively). Compared to free GC, in GC-$Al_{12}X$ complexes the O6(G)···N4(C) bond is weakened and N2(G)···O2(C) is reinforced, whereas N1(G)···N3(C) changes only slightly. Clearly, depending on the nature of the metal clusters, the intermolecular H bonds of BPs can be reinforced, weakened, or even altered remarkably. This conclusion is further confirmed by the computational comparisons between the base–base interaction energies for BP-$Al_{12}X$ complexes and those for the free BPs (Table 2).

Electronic properties

Charge distributions and redox properties

Detailed analyses of NBO charge distributions were performed (Table 3). Clearly, $Al_{12}X$ clusters have negative charges in all complexes except C-$Al_{12}P$. Considerable charge transfers occur in all complexes, with the smallest amount of 0.16 *e* in T-$Al_{12}P$. Surprisingly, the largest charge transfer occurs in the C-$Al_{12}P$ complex, in which the C moiety obtains a substantial amount of negative charge (−0.51 *e*) from the $Al_{12}P$.

We then computed the vertical and adiabatic ionization potentials (VIPs, AIPs) of the individual bases and BPs. The IP values (VIPs 8.58, 9.33, 8.30, and 9.06 eV for A, T, G and C, respectively; the corresponding AIP values are 8.32, 9.02, 7.87 and 8.92 eV) have the order G < A < C < T, which agrees very well with previous high accuracy computations [61]. Thus, in the case of AT-$Al_{12}X$, the T moiety can gain an electron from A and become negatively charged. However, in the GC-$Al_{12}X$ complex, G loses an electron more easily than C, so G contributes most of the negative charge localized on the $Al_{12}X$. GC has a VIP of 7.56 eV and AIP of 7.14 eV, smaller than those of AT (VIP 8.35 eV, AIP 8.00 eV). Thus, $Al_{12}X$ can obtain more electrons (ca. 0.1 *e*, Table 3) from GC than from AT.

In addition, we computed the vertical and adiabatic electron affinities (VEAs, AEAs) for the $Al_{12}X$ clusters. The EA values (VEAs 3.23, 1.43, 2.28 and 1.44 eV, respectively, for Al_{13}, $Al_{12}C$, $Al_{12}N$ and $Al_{12}P$; the corresponding AEA values are 3.49, 1.44, 2.28 and 1.45 eV) have the order $Al_{12}C < Al_{12}P < Al_{12}N < Al_{13}$. Thus, we can expect that both T and AT have small affinities to bind $Al_{12}C$, which is in line with the above discussions of ΔG_b. Moreover, we can also anticipate that Al_{13} can gain some electrons from the BPs due to its large EA, which was confirmed by the computed NBO charge (Table 3), although all four $Al_{12}X$ clusters obtain electrons from the BPs, regardless of whether the $Al_{12}X$ cluster is electron deficient or abundant.

On the other hand, the Al atom(s) bound to the bases/BPs all exhibit positive charge (Figs. 2, 3). For example, the charges on the relevant Al atoms are 0.24, 0.14, 0.12 and 0.13 *e* in A-Al_{13}, A-$Al_{12}C$, A-$Al_{12}N$ and A-$Al_{12}P$, respectively. Thus, although the whole NP can attract electrons from the base, locally the Al atom attached to

Table 3 Total NBO charges (*e*) in the base/BP-$Al_{12}X$ complexes computed at the M05-2X/6-311+G* level of theory

	Base/BP−Al_{13}		Base/BP−$Al_{12}C$		Base/BP−$Al_{12}N$		Base/BP−$Al_{12}P$	
	Base/BP	Al_{13}	Base/BP	$Al_{12}C$	Base/BP	$Al_{12}N$	Base/BP	$Al_{12}P$
A	0.20	−0.20	0.20	−0.20	0.20	−0.20	0.19	−0.19
T	0.17	−0.17	0.17	−0.17	0.17	−0.17	0.16	−0.16
G	0.17	−0.17	0.18	−0.18	0.17	−0.17	0.17	−0.17
C	0.19	−0.19	0.19	−0.19	0.19	−0.19	−0.51	0.51
A(AT)	0.22	−0.20	0.20	−0.20	0.20	−0.20	0.41	−0.19
T(AT)	−0.02		0.00		0.00		−0.22	
G(GC)	0.24	−0.33	0.24	−0.32	0.24	−0.33	0.24	−0.32
C(GC)	0.09		0.08		0.09		0.08	

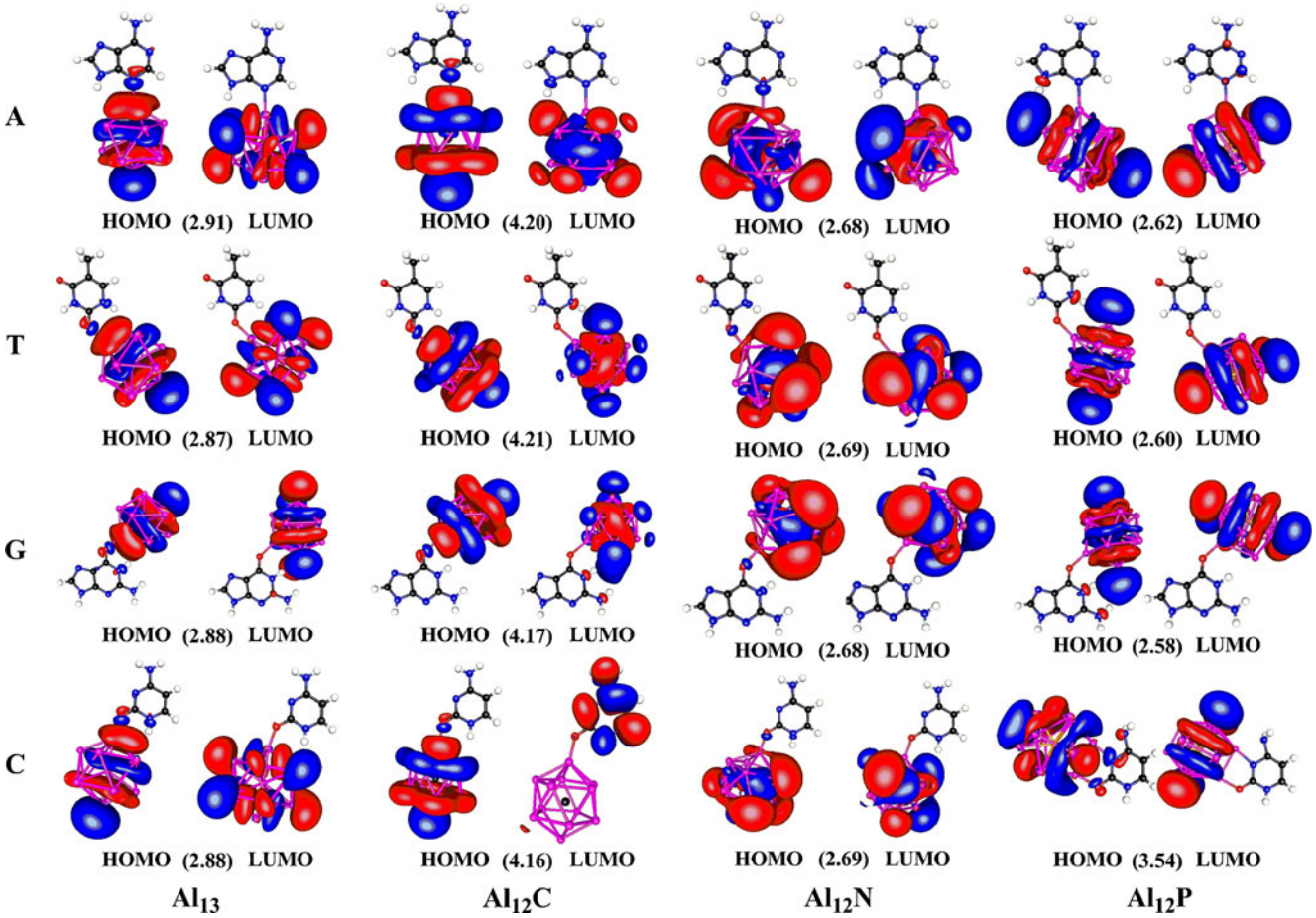

Fig. 4 Plots of the frontier orbitals for the base–$Al_{12}X$ complexes and the corresponding HOMO−LUMO gap energies (eV, in parentheses) computed at the M05-2X/6-311+G* level of theory

the base is positively charged, due mainly to the connecting electronegative O or N atom.

For complexes with both bases and BPs, the charges on the inner X atoms change little for the same $Al_{12}X$ (Figs. 2, 3). These complexes manifest a large electronic shielding effect of the outer Al shells. From the geometrical parameters and the charge distributions of the studied complexes, we conclude that all $Al_{12}X$ NPs are coordinated

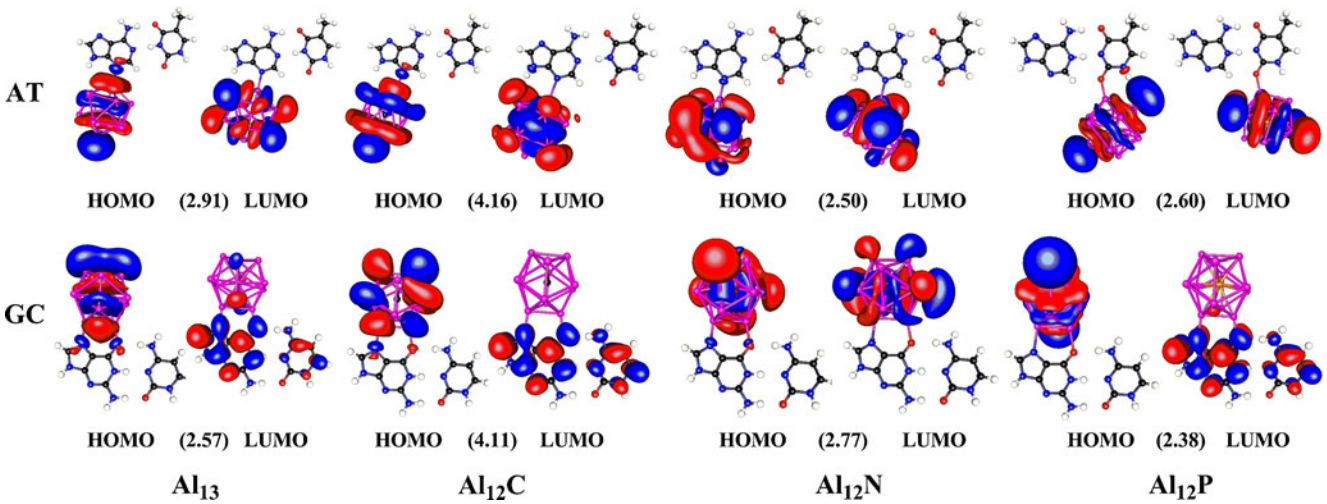

Fig. 5 Plots of the frontier orbitals for the BP-$Al_{12}X$ complexes and the corresponding HOMO−LUMO gap energies (eV, in parentheses) computed at the M05-2X/6-311+G* level of theory

to bases and BPs through both covalent bonds and electrostatic interactions.

Frontier molecular orbitals

To derive useful information about the reactivity of the complexes under study, we plotted their frontier molecular orbitals, especially the highest occupied molecular orbital (HOMO) and the lowest unoccupied molecular orbital (LUMO). The HOMOs and LUMOs are localized around the $Al_{12}X$ NP in almost all of the base–$Al_{12}X$ complexes (Fig. 4) with the exception of C-$Al_{12}C$, whose LUMO locates mainly on the cytosine moiety. Thus, oxidation as well as reduction reactions occur mostly on the metal clusters.

Similarly, most of the frontier orbitals of the BP-$Al_{12}X$ complexes locate on the Al clusters. The exceptions are the LUMOs in GC-$Al_{12}X$ (X = Al, C and P), which are localized mainly on the BPs (Fig. 5). Furthermore, all of the base/BP-$Al_{12}X$ complexes have sizable HOMO−LUMO gap energies (ranging from 2.58 to 4.21 eV and 2.38 to 4.16 eV for base–$Al_{12}X$ and BP-$Al_{12}X$, respectively), suggesting high kinetic stabilities.

Implications to the nanotoxicity of aluminum clusters

Our computations reveal that the $Al_{12}X$ clusters have very strong interactions with DNA bases and base pairs (To confirm this, ΔG_b values at higher temperatures (298.15–318.15 K) and BSSE-corrected binding energies were also estimated (summarized in Fig. S1 and Table S3, respectively, see Supporting Information). Notably, the typically highly stable magic cluster $Al_{12}C$ is also very reactive and interacts strongly with DNA, and the redox properties of the $Al_{12}X$ clusters do not have significant effects. It is the rather robust interaction between the surface Al atoms and the elements with high electronegativity (N and O) that binds the $Al_{12}X$ cluster and DNA. Thus, it is expected that larger Al NPs also tightly attach to DNA. Such interactions will most likely cause structural damage and electronic property changes in the DNA, and consequently lead to adverse effects on DNA function.

Conclusions

In summary, we performed a detailed theoretical study of complexes composed of DNA bases/BPs and $Al_{12}X$ (X = Al, C, N and P) clusters by means of DFT computations. All of these $Al_{12}X$ clusters attach tightly to the bases/BPs with negative binding Gibbs free energies due to the strong interactions between the outer Al atoms and the related binding sites, but the different redox properties of $Al_{12}X$ NPs have an insignificant effect. All four NPs (one is closed shell, three are open shell) can attract electrons from the BPs. The intermolecular H bonds of the BPs can be reinforced, weakened, or altered markedly depending on the nature of the metal cluster. All these findings suggest that the bound $Al_{12}X$ clusters, as well as larger Al nanoparticles, can affect the structure and stability of DNA, and may cause negative effects on its function. We hope this study sheds light on nanotoxicology research and stimulates more theoretical studies on the toxicities of NPs.

Acknowledgments This research has been supported in China by the National Science Foundation of China (Grant No. 20921004) and in the United States by the National Science Foundation (Grant EPS-1010094), the Institutional Research Fund of University of Puerto Rico, and the US Environmental Protection Agency (EPA Grant No. RD-83385601). We thank Computational Center for Nanotechnology Innovations (CCNI) and TeraGrid for providing computational resources.

References

1. Fischer HC, Chan WC (2007) Nanotoxicity: the growing need for in vivo study. Curr Opin Biotechnol 18:565–571
2. Lubick N (2008) Risks of nanotechnology remain uncertain. Environ Sci Technol 42:1821–1824
3. Buzea C, Pacheco II, Robbie K (2007) Nanomaterials and nanoparticles: sources and toxicity. Biointerphases 2:MR17–MR71
4. Ray PC, Yu H, Fu PP (2009) Toxicity and environmental risks of nanomaterials: challenges and future needs. J Environ Sci Health C Environ Carcinog Ecotoxicol Rev 27:1–35
5. Bouwmeester H, Dekkers S, Noordam MY, Hagens WI, Bulder AS, De Heer C, Ten Voorde SECG, Wijnhoven SWP, Marvin HJP, Sips AJAM (2009) Review of health safety aspects of nanotechnologies in food production. Regul Toxicol Pharm 53:52–62
6. Jones CF, Grainger DW (2009) In vitro assessments of nanomaterial toxicity. Adv Drug Deliv Rev 61:438–456
7. Hillegass JM, Arti S, Lathrop SA, MacPherson MB, Fukagawa NK, Mossman BT (2010) Assessing nanotoxicity in cells in vitro. Wiley Interdiscip Rev Nanomed Nanobiotechnol 2:219–231
8. Dhawan A, Sharma V (2010) Toxicity assessment of nanomaterials: methods and challenges. Anal Bioanal Chem 398:589–605
9. Hu YL, Gao JQ (2010) Potential neurotoxicity of nanoparticles. Int J Pharm 394:115–121
10. Fadeel B, Garcia-Bennett AE (2010) Better safe than sorry: Understanding the toxicological properties of inorganic nanoparticles manufactured for biomedical applications. Adv Drug Deliv Rev 62:362–374
11. Aillon KL, Xie Y, El-Gendy N, Berkland CJ, Forrest ML (2009) Effects of nanomaterial physicochemical properties on in vivo toxicity. Adv Drug Deliv Rev 61:457–466
12. Shvedova AA, Kagan VE, Fadeel B (2010) Close encounters of the small kind: adverse effects of man-made materials interfacing with the nano-cosmos of biological systems. Annu Rev Pharmacol Toxicol 50:63–88
13. Balbus JM, Maynard AD, Colvin VL, Castranova V, Daston GP, Denison RA, Dreher KL, Goering PL, Goldberg AM, Kulinowski KM, Monteiro-Riviere NA, Oberdörster G, Omenn GS, Pinkerton

KE, Ramos KS, Rest KM, Sass JB, Silbergeld EK, Wong BA (2007) Meeting report: hazard assessment for nanoparticles—report from an interdisciplinary workshop. Environ Health Perspect 115:1654–1659
14. Ostrowski AD, Martin T, Conti J, Hurt I, Harthorn BH (2009) Nanotoxicology: characterizing the scientific literature, 2000-2007. J Nanopart Res 11:251–257
15. Bosi S, Feruglio L, Ros TD, Spalluto G, Gregoretti B, Terdoslavich M, Decorti G, Passamonti S, Moro S, Prato M (2004) Hemolytic effects of water-soluble fullerene derivatives. J Med Chem 47:6711–6715
16. Zhao X, Striolo A, Cummings PT (2005) C_{60} binds to and deforms nucleotides. Biophys J 89:3856–3862
17. Zhao X (2008) Interaction of C_{60} derivatives and ssDNA from simulations. J Phys Chem C 112:8898–8906
18. Shukla MK, Leszczynski J (2009) Fullerene (C_{60}) forms stable complex with nucleic acid base guanine. Chem Phys Lett 469:207–209
19. Shukla MK, Dubey M, Zakar E, Namburu R, Czyznikowska Z, Leszczynski J (2009) Interaction of nucleic acid bases with single-walled carbon nanotube. Chem Phys Lett 480:269–272
20. Shukla MK, Dubey M, Zakar E, Namburu R, Leszczynski J (2010) Interaction of nucleic acid bases and Watson-Crick base pairs with fullerene: computational study. Chem Phys Lett 493:130–134
21. Shukla MK, Dubey M, Zakar E, Namburu R, Leszczynski J (2010) Density functional theory investigation of interaction of zigzag (7,0) single-walled carbon nanotube with Watson-Crick DNA base pairs. Chem Phys Lett 496:128–132
22. Mazzuca D, Russo N, Toscano M, Grand A (2006) On the interaction of bare and hydrated aluminum ion with nucleic acid bases (U, T, C, A, G) and monophosphate nucleotides (UMP, dTMP, dCMP, dAMP, dGMP). J Phys Chem B 110:8815–8824
23. Bedrov D, Smith GD, Davande H, Li L (2008) Passive transport of C_{60} fullerenes through a lipid membrane: a molecular dynamics simulation study. J Phys Chem B 112:2078–2084
24. Shang J, Ratnikova TA, Anttalainen S, Salonen E, Ke PC, Knap HT (2009) Experimental and simulation studies of a real-time polymerase chain reaction in the presence of a fullerene derivative. Nanotechnology 20:415101
25. Redmill PS, McCabe C (2010) Molecular dynamics study of the behavior of selected nanoscale building blocks in a gel-phase lipid bilayer. J Phys Chem B 114:9165–9172
26. Perl DP, Gajdusek DC, Garruto RM, Yanagihara RT, Gibbs CJ (1982) Intraneuronal aluminum accumuation in amyotrophic lateral sclerosis and Parkinsonism-dementia of Guam. Science 217:1053–1055
27. De Broe ME, Coburn JW (1990) Aluminium and renal failure. Dekker, New York
28. Guillard O, Fauconneau B, Olichon D, Dedieu G, Deloncle R (2004) Hyperaluminemia in a woman using an aluminum-containing antiperspirant for 4 years. Am J Med 117:956–959
29. Foncin JF (1987) Alzheimer's disease and aluminum. Nature 326:136
30. Kawahara M (2005) Effects of aluminum on the nervous system and its possible link with neurodegenerative diseases. J Alzheimers Dis 8:171–182
31. Braydich-Stolle LK, Speshock JL, Castle A, Smith M, Murdock RC, Hussain SM (2010) Nanosized aluminum altered immune function. ACS Nano 4:3661–3670
32. Pedersen DB, Simard B, Martinez A, Moussatova A (2003) Stabilization of an unusual tautomer of guanine: photoionization of Al-guanine and Al-guanine-$(NH_3)_n$. J Phys Chem A 107:6464–6469
33. Frisch MJ et al (2004) Gaussian 03, Gaussian, Inc., Wallingford CT
34. Pedersen DB, Zgierski MZ, Denommee S, Simard B (2002) Photoinduced charge-transfer dehydrogenation in a gas-phase metal-DNA base complex: Al-cytosine. J Am Chem Soc 124:6686–6692
35. De Heer WA (1993) The physics of simple metal clusters: experimental aspects and simple models. Rev Mod Phys 65:611–676
36. Khanna SN, Jena P (1992) Assembling crystals from clusters. Phys Rev Lett 69:1664–1667
37. Gong XG, Kumar V (1993) Enhanced stability of magic clusters: a case study of icosahedral $Al_{12}X$, X = B, Al, Ga, C, Si, Ge, Ti, As. Phys Rev Lett 70:2078–2081
38. Kumar V, Bhattacharjee S, Kawazoe Y (2000) Silicon-doped icosahedral, cuboctahedral, and decahedral clusters of aluminum. Phys Rev B 61:8541–8547
39. Akutsu M, Koyasu K, Atobe J, Hosoya N, Miyajima K, Mitsui M, Nakajima A (2006) Experimental and theoretical characterization of aluminum-based binary superatoms of $Al_{12}X$ and their cluster salts. J Phys Chem A 110:12073–12076
40. Wang B, Zhao J, Shi D, Chen X, Wang G (2005) Density-functional study of structural and electronic properties of Al_nN (n=2–12) clusters. Phys Rev A 72:023204
41. Zhao Y, Schultz NE, Truhlar DG (2006) Design of density functionals by combining the method of constraint satisfaction with parametrization for thermochemistry, thermochemical kinetics, and noncovalent interactions. J Chem Theor Comput 2:364–382
42. Zhao Y, Truhlar DG (2008) Density functionals with broad applicability in chemistry. Acc Chem Res 41:157–167
43. Henry DJ, Varano A, Yarovsky I (2008) Performance of numerical basis set DFT for aluminum clusters. J Phys Chem A 112:9835–9844, and references therein
44. Tomasi J, Mennucci B, Cammi R (2005) Quantum mechanical continuum solvation models. Chem Rev 105:2999–3094
45. Reed AE, Curtiss LA, Weinhold F (1988) Intermolecular interactions from a natural bond orbital donor-acceptor viewpoint. Chem Rev 88:899–926
46. Boys SF, Bernardi F (1970) The calculation of small molecular interactions by the differences of separate total energies. Some procedures with reduced errors. Mol Phys 19:553–566
47. Vázquez M-V, Martínez A (2008) Theoretical study of cytosine-Al, cytosine-Cu and cytosine-Ag (neutral, anionic and cationic). J Phys Chem A 112:1033–1039
48. Laaksonen L (1992) A graphics program for the analysis and display of molecular dynamics trajectories. J Mol Graph 10:33–34
49. Bergman DL, Laaksonen L, Laaksonen A (1997) Visualization of solvation structure in liquid mixtures. J Mol Graph Model 15:301–306
50. Lippert B (2000) Multiplicity of metal ion binding patterns to nucleobases. Coord Chem Rev 200–202:487–516
51. Hud NV (2009) Nucleic acid–metal ion interactions. RSC, Cambridge
52. Krasnokutski SA, Lei Y, Lee JS, Yang DS (2008) Pulsed-field ionization photoelectron and IR-UV resonant photoionization spectroscopy of Al-thymine. J Chem Phys 129:124309
53. Moussatova A, Vázquez M-V, Martínez A, Dolgounitcheva O, Zakrzewski VG, Ortiz JV, Pedersen DB, Simard B (2003) Theoretical study of the structure and bonding of a metal-DNA base complex: Al-guanine. J Phys Chem A 107:9415–9421
54. Robertazzi A, Platts JA (2005) Hydrogen bonding and covalent effects in binding of cisplatin to purine bases: ab initio and atoms in molecules studies. Inorg Chem 44:267–274
55. Baker ES, Manard MJ, Gidden J, Bowers MT (2005) Structural analysis of metal interactions with the dinucleotide duplex, dCG. dCG, using ion mobility mass spectrometry. J Phys Chem B 109:4808–4810

56. Pelmenschikov A, Zilberberg I, Leszczynski J, Famulari A, Sironi M, Raimondi M (1999) cis-$[Pt(NH_3)_2]^{2+}$ coordination to the N7 and O6 sites of a guanine-cytosine pair: disruption of the Watson-Crick H-bonding pattern. Chem Phys Lett 314:496–500
57. Zilberberg IL, Avdeev VI, Zhidomirov GM (1997) Effect of cisplatin binding on guanine in nucleic acid: an ab initio study. J Mol Struct THEOCHEM 418:73–81
58. Robertazzi A, Platts JA (2005) Binding of transition metal complexes to guanine and guanine–cytosine: hydrogen bonding and covalent effects. J Biol Inorg Chem 10:854–866
59. Mo Y (2006) Probing the nature of hydrogen bonds in DNA base pairs. J Mol Model 12:665–672
60. Quinn JR, Zimmerman SC, Del Bene JE, Shavitt I (2007) Does the A•T or G•C base-pair possess enhanced stability? Quantifying the effects of CH•••O interactions and secondary interactions on base-pair stability using a phenomenological analysis and ab initio calculations. J Am Chem Soc 129:934–941
61. Roca-Sanjuán D, Rubio M, Merchán M, Serrano-Andrés L (2006) Ab initio determination of the ionization potentials of DNA and RNA nucleobases. J Chem Phys 125:084302